

# Single-crystal parallel-mode EPR spectroscopy of an $S=6$ ground-state transition-metal cluster

Stergios Piligkos,<sup>1</sup> David Collison,<sup>1</sup> Vasily S. Oganesyan,<sup>2</sup> Gopalan Rajaraman,<sup>1</sup> Grigore A. Timco,<sup>1</sup> Andrew J. Thomson,<sup>2</sup> Richard E. P. Winpenny,<sup>1</sup> and Eric J. L. McInnes<sup>1,\*</sup>

<sup>1</sup>Department of Chemistry, The University of Manchester, Oxford Road, Manchester M13 9PL, United Kingdom

<sup>2</sup>School of Chemical Sciences and Pharmacy, University of East Anglia, Norwich NR4 7TJ, United Kingdom

(Received 16 January 2004; revised manuscript received 20 February 2004; published 28 April 2004)

We present a parallel-mode EPR study of a very high-spin ground-state cluster complex  $[\text{Cr}_{12}\text{O}_9(\text{OH})_3(\text{O}_2\text{CCMe}_3)_{15}]$ , where Me indicates the methyl group. This high-symmetry ( $D_3$ ) molecule has a well-isolated  $S=6$  ground state characterized by  $D=+0.088 \text{ cm}^{-1}$ ,  $E=0$ ,  $g_{zz}=1.965$ ,  $g_{xx}=g_{yy}=1.960$ . Low-temperature (5 K) single-crystal and powder parallel- and perpendicular-mode EPR spectra are presented. The forms of the spectra are discussed with respect to the composition of the wave functions as a function of the angle of the static magnetic field to the molecular Z axis, the selection rules of the two excitation modes, and the resultant transition probabilities. This is the largest spin state studied by parallel mode EPR spectroscopy to date, and the results demonstrate the applicability of parallel-mode EPR to high-spin ground-state molecular clusters such as single-molecule magnets.

DOI: 10.1103/PhysRevB.69.134424

PACS number(s): 76.30.-v, 36.40.-c, 75.50.Xx

## INTRODUCTION

Continuous-wave electron paramagnetic resonance (EPR) spectroscopy involves application of the oscillating magnetic component of the incident microwave radiation ( $B_1$ ) perpendicular to the static magnetic field ( $B_0$ ).<sup>1</sup> This leads to the spin selection rule  $\Delta M_S = \pm 1$ . In *parallel-mode* EPR spectroscopy,  $B_1$  is applied parallel to  $B_0$ , and it is possible to observe  $\Delta M_S = 0$  transitions. Parallel-mode EPR has been exploited to great effect to study integer-spin systems in biology,<sup>2</sup> where, typically, zero-field splittings (ZFSs) are larger than the microwave quantum at X-band (ca.  $0.3 \text{ cm}^{-1}$ ). For example, there are many metalloenzymes that have high-spin Fe(II) at the active site. The non-Kramers  $S=2$  ground-state multiplet is split by the axial ZFS parameter  $D$  into degenerate sets of  $M_S = \pm 2$ ,  $\pm 1$ , and 0. In this case, perpendicular-mode EPR transitions can be excited only at very high magnetic fields, beyond the range of typical X-band fields. However, in parallel mode, transitions are often observed within the “ $M_S = \pm 2$ ” doublet, where the  $M_S = 0$  and  $\pm 2$  states are mixed by a nonzero rhombic term ( $E$ ) in the spin Hamiltonian, allowing transitions within the doublet.<sup>3</sup> For the same reason, parallel-mode EPR has also found great use in the study of integer-spin metal clusters in biology, for example in iron-sulfur proteins<sup>4</sup> and the Mn cluster in photosystem II.<sup>5</sup>

We are interested in transition-metal clusters with very high ground-state spins, because these can behave as “single-molecule magnets” (SMMs).<sup>6</sup> SMMs show slow relaxation of magnetization at low temperature because there is an energy barrier to loss of magnetization due to a significant negative ZFS ( $D$ ) of the spin ground state  $S$ .<sup>6(b)</sup> This removes the degeneracy of the  $M_s$  spin states and, because  $D$  is negative,  $M_s=0$  is highest in energy at zero-field, while  $M_s=\pm S$  are lowest in energy, with the former at an energy of  $|D|S_z^2$  with respect to the latter. This provides the energy barrier to loss of magnetization for integer-spin systems [for half-integer spins the barrier is given by  $|D|(S_z^2 - 1/4)$ ].

Thus, SMMs display a molecular magnetic hysteresis and therefore have potential applications in magnetic memory devices. It has also been proposed that such molecules could be used in quantum computing, with the required superposition of spin eigenstates achieved either via a complicated sequence of perpendicular and parallel mode EPR pulses,<sup>7</sup> or via a weak exchange interaction (“exchange biasing”) between discrete dimers of clusters.<sup>8</sup>

However, while perpendicular-mode EPR of such high-spin clusters has been reported frequently,<sup>9</sup> parallel-mode studies have not been pursued. Parallel-mode studies have been reported on high-spin biological FeS clusters ( $S$  up to 9/2).<sup>4</sup> In this work we report a parallel-mode EPR study of a single crystal of the  $S=6$  ground state cluster  $[\text{Cr}_{12}\text{O}_9(\text{OH})_3(\text{O}_2\text{CCMe}_3)_{15}]$ ,<sup>10</sup> where Me indicates the methyl group, “ $\text{Cr}_{12}$ ” (Fig. 1) allowing a detailed comparison of perpendicular and parallel modes, including orientation dependence, of a molecule with a very high-spin ground state. This is the highest-spin state studied by parallel-mode EPR to date to our knowledge.

## EXPERIMENT

The preparation of  $\text{Cr}_{12}$  has been reported previously.<sup>10</sup> Single crystals were grown by slow evaporation of *n*-propanol solutions to give  $1 \times 1 \times 0.1 \text{ mm}^3$  dark green rhomb shaped crystals of  $[\text{Cr}_{12}\text{O}_9(\text{OH})_3(\text{O}_2\text{CCMe}_3)_{15}] \cdot \text{PrOH}$ , where Pr indicates the propyl group. The crystals lose solvent on prolonged exposure to air, but are indefinitely stable when coated in grease. The unit cell details are  $R\bar{3}2$ , rhombohedral,  $a=b=18.5902(16) \text{ \AA}$ ,  $c=36.0230(50) \text{ \AA}$ . The  $\text{Cr}_{12}$  molecules all lie on 32 sites, thus imposing crystallographic  $D_3$  point symmetry, with the molecular Z axes (the  $C_3$  rotation axes) aligned parallel with the crystal  $c$  axis. The  $c$  axis lies along the body diagonal of the long axis of the crystal.

EPR spectra were measured on a Bruker ESP 300E cw EPR spectrometer equipped with a Bruker 4116DM X-band dual mode resonator and Oxford Instruments ESR9 cryostat.

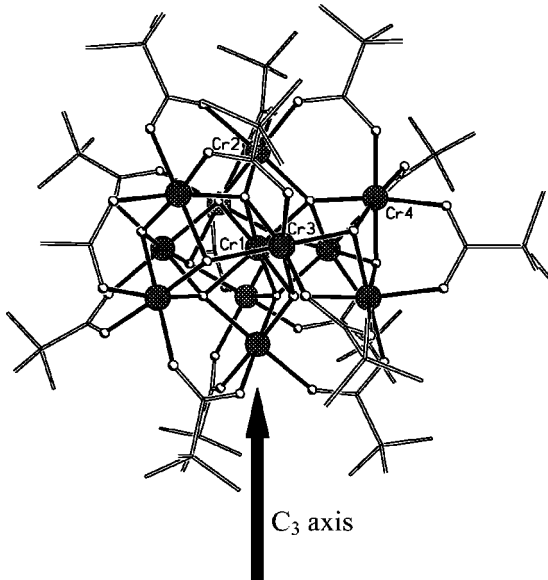


FIG. 1. The structure of  $\text{Cr}_{12}$  in the crystal, viewed perpendicular to the principal axis of the molecule. The  $C_3$  axis passes through  $\text{Cr}1$  and  $\text{Cr}2$ , while the  $C_2$  axes pass through  $\text{Cr}1$  and  $\text{Cr}3$  (and its symmetry equivalents).

The resonator tuned at 9.65 and 9.43 GHz for perpendicular and parallel modes, respectively. Well-resolved spectra from the  $S=6$  ground state are observed only below ca. 30 K, where this state is populated.<sup>11</sup> All spectra in this work were measured at 5 K. Single-crystal samples were mounted on quartz studs with machined faces to allow orientation and rotation in known crystallographic planes. The crystals could be aligned along, e.g., the  $c$  axis by exploiting the spectral properties and known<sup>11</sup> spin Hamiltonian parameters (see below). Thus, spectra were measured at regular increments in the molecular  $ZX$  plane (see below). Spectrum simulations were performed with in-house software.<sup>2(a)</sup>

## RESULTS AND DISCUSSION

$\text{Cr}_{12}$  is a dodecametallic Cr(III) cluster.<sup>11</sup> The structure consists of a centered trigonal prism of Cr(III) ions, capped on each rectangular and triangular face by further Cr(III) ions (see Fig. 1). The cluster has crystallographically imposed  $D_3$  point symmetry. The  $C_3$  axis of the molecule lies along the vector defined by the central Cr(III) ion ( $\text{Cr}1$ ) and the two triangular face caps ( $\text{Cr}2$  and symmetry equivalent). Magnetic exchange, via bridging oxide and hydroxide groups, leads to an  $S=6$  spin ground state.<sup>11</sup> This ground state is populated exclusively below ca. 10 K, as judged by the saturation of  $\chi T$  vs  $T$  below this temperature ( $\chi$  = molar magnetic susceptibility).<sup>11</sup> The ground state can be described by the spin Hamiltonian

$$\hat{H} = \beta \tilde{\mathbf{g}} \cdot \mathbf{B}_0 \cdot \hat{\mathbf{S}} + D \left[ \hat{S}_z^2 - \frac{1}{3} S(S+1) \right]. \quad (1)$$

The first term of this equation is the electronic Zeeman effect and the second term is the uniaxial anisotropy due to ZFS. The rhombic zero-field splitting parameter  $E$  is necessarily

zero given that the cluster has  $D_3$  point symmetry, and we have obtained no evidence for higher-order terms in  $S$ . Additionally, no observable effects of intermolecular exchange were found and this compound can be considered to be magnetically dilute. The spin Hamiltonian parameters have been established by multifrequency EPR on powder samples:<sup>11</sup>  $S = 6$ ,  $g_{zz} = 1.965$ ,  $g_{xx} = g_{yy} = 1.960$ ,  $D = +0.088 \text{ cm}^{-1}$  (the sign of  $D$  comes from modeling depopulation changes observed in 180 GHz EPR measurements). The principal axis of the axial  $\mathbf{D}$  tensor is required by symmetry to be parallel to the  $C_3$  axis of the molecule in  $D_3$  point symmetry. Because the molecule lies on a 32 site in the  $R\bar{3}2$  space group, there is only one magnetically distinct molecule at all orientations of the crystal with respect to the magnetic field. This high crystal and molecular symmetry of the cluster, combined with the magnitude of  $D$  (perpendicular-*and* parallel-mode spectra can be observed), make  $\text{Cr}_{12}$  an ideal case study for the parallel-mode EPR spectroscopy of high-spin cage complexes. Although the positive sign of  $D$  means that  $\text{Cr}_{12}$  is not a single-molecule magnet, all the arguments below are equally valid for a negative  $D$  value.

Figure 2 shows representative examples of the angular variation of the single-crystal X-band EPR spectra of  $\text{Cr}_{12}$  recorded in both perpendicular and parallel modes. Intense perpendicular-mode spectra are observed for all orientations of the crystal (molecule) with respect to the static magnetic field, whereas there is significant intensity in parallel mode only when the magnetic field is not oriented along the molecular  $Z$  axis.

The orientation of the static magnetic field ( $B_0$ ) with respect to the molecular axis system ( $X, Y, Z$ ) can be defined by the polar angle  $\theta$  between the  $Z$  molecular axis and the static magnetic field because the axial symmetry of the molecule ensures that all orientations with respect to the azimuthal angle  $\phi$  are equivalent. The numerically special position  $\phi=0^\circ$  can be considered for simplicity.

In the case of perpendicular-mode EPR the incident microwave radiation ( $B_1$ ) is applied perpendicular to the static magnetic field ( $B_0$ ). If  $B_0$  forms an angle  $\theta$  with  $Z$ , then the orientation of  $B_1$  with respect to this axis will be defined by an angle of  $\theta + \pi/2$ .

The perturbation Hamiltonian in this case will be of the form

$$\begin{aligned} \hat{H}_{pert} &= \beta \mathbf{B}_1 \cdot \tilde{\mathbf{g}} \cdot \hat{\mathbf{S}}, \\ \hat{H}_{pert} &= \beta \cdot \mathbf{B}_1 \left[ g_{xx} \cdot \hat{S}_x \cdot \cos(\theta) + g_{zz} \cdot \hat{S}_z \cdot \cos\left(\theta + \frac{\pi}{2}\right) \right], \\ \hat{H}_{pert} &= \beta \cdot \mathbf{B}_1 [g_{xx} \cdot \hat{S}_x \cdot \cos(\theta) - g_{zz} \cdot \hat{S}_z \cdot \sin(\theta)]. \end{aligned}$$

For the two limiting cases ( $\theta=0^\circ$  and  $\theta=90^\circ$ ), this gives the following results.

For  $\theta=0^\circ$ ,

$$\hat{H}_{pert} = \beta \cdot \mathbf{B}_1 \cdot g_{xx} \cdot \hat{S}_x. \quad (2)$$

This perturbation Hamiltonian has nonzero matrix elements when

$$\langle \varphi(i) | \hat{S}_{\pm} | \varphi(j) \rangle \neq 0, \quad (3)$$

where  $\beta$  is the electronic Bohr magneton,  $\tilde{\mathbf{g}}$  is the electron  $g$  matrix with the principal components  $g_{xx}$ ,  $g_{yy}$ ,  $g_{zz}$ ,  $\hat{S}_+$  and  $\hat{S}_-$  are the raising and lowering spin operators, respectively, and  $|\varphi(i)\rangle$  are wave functions obtained after diagonalization of Eq. (1). Since at this orientation the wave functions  $|\varphi(i)\rangle$  are pure spin states  $|S, M_S\rangle$  the two energy levels involved in a transition must be described by wave functions differing by  $\pm 1$  in the quantum number  $M_S$  in order to have significant transition probabilities. This is the origin of the  $\Delta M_S = \pm 1$  selection rule in perpendicular-mode EPR spectroscopy.

For  $\theta = 90^\circ$ ,

$$\hat{H}_{pert} = -\beta \cdot \mathbf{B}_1 \cdot g_{zz} \cdot \hat{S}_z \quad (4)$$

which means the nonzero matrix elements are now of the type

$$\langle \varphi(i) | \hat{S}_z | \varphi(j) \rangle \neq 0. \quad (5)$$

Transitions of significant probability are then observed between energy levels described by wave functions of the same  $M_S$  quantum number, i.e., the selection rule becomes  $\Delta M_S = 0$ , which can become allowed when the wave functions are mixed such that they contain admixtures of the same  $M_S$  states (see below).

In the case of parallel-mode EPR the incident microwave radiation ( $B_1$ ) is applied parallel to the static magnetic field ( $B_0$ ). Both  $B_0$  and  $B_1$  form the same angle  $\theta$  with respect to the  $Z$  molecular axis.

The perturbation Hamiltonian in the case of the parallel mode will be of the form

$$\hat{H}_{pert} = \beta \cdot \mathbf{B}_1 \cdot \tilde{\mathbf{g}} \cdot \hat{S},$$

$$\hat{H}_{pert} = \beta \cdot \mathbf{B}_1 \left[ g_{xx} \cdot \hat{S}_x \cdot \cos\left(\frac{\pi}{2} - \theta\right) + g_{zz} \cdot \hat{S}_z \cdot \cos(\theta) \right],$$

$$\hat{H}_{pert} = \beta \cdot \mathbf{B}_1 [g_{xx} \cdot \hat{S}_x \cdot \sin(\theta) + g_{zz} \cdot \hat{S}_z \cdot \cos(\theta)].$$

For the two limiting cases ( $\theta = 0^\circ$  and  $\theta = 90^\circ$ ), this gives the following.

For  $\theta = 0^\circ$ ,

$$\hat{H}_{pert} = \beta \cdot \mathbf{B}_1 \cdot g_{zz} \cdot \hat{S}_z \quad (6)$$

giving nonzero matrix elements of type (5). Transitions of significant probability are then observed between energy levels described by wave functions of the same  $M_S$  quantum number.

For  $\theta = 90^\circ$ ,

$$\hat{H}_{pert} = \beta \cdot \mathbf{B}_1 \cdot g_{xx} \cdot \hat{S}_x. \quad (7)$$

This has nonzero matrix elements when Eq. (3) is satisfied. Thus the two energy levels involved in a transition must be described by wave functions differing by  $\pm 1$  in  $M_S$ .

With the static magnetic field parallel to  $Z$  ( $\theta = 0^\circ$ ), an eight-line multiplet is observed for  $\text{Cr}_{12}$  in perpendicular-

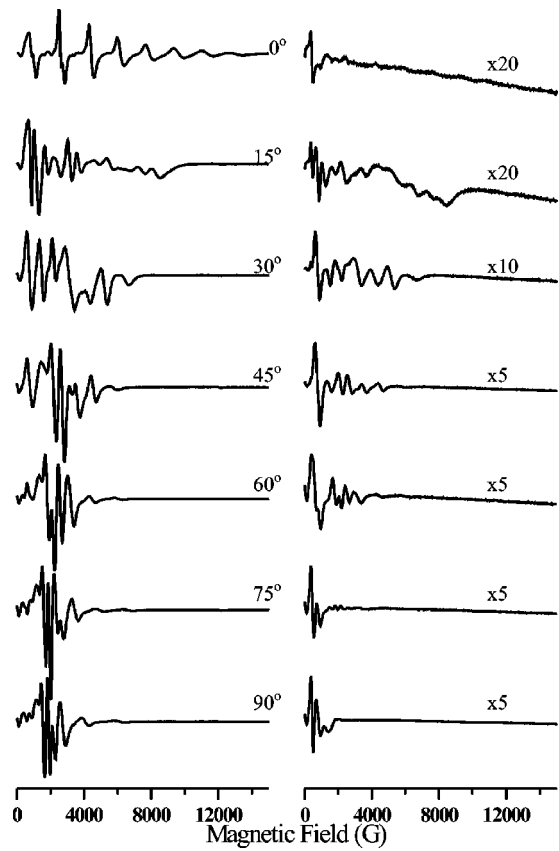


FIG. 2.  $X$ -band EPR spectra (at 5 K and  $\nu = 9.62$  GHz) of a single crystal of  $\text{Cr}_{12}$  in the  $ZX$  molecular plane, recorded in perpendicular (left column) and parallel mode (right column):  $\theta = 0^\circ$ ,  $15^\circ$ ,  $30^\circ$ ,  $45^\circ$ ,  $60^\circ$ ,  $75^\circ$ , and  $90^\circ$  where  $\theta$  is the angle with respect to the molecular  $Z$  axis. The spectra were recorded under identical conditions and the parallel-mode spectra have been scaled by the factors shown. Note there is slight “leakage” between the two modes as witnessed by the very weak (perpendicular mode) transitions observed in the parallel mode spectrum at  $0^\circ$ .

mode EPR (Fig. 2), with neighboring transitions separated by approximately  $2D$  (ca. 1800 G in units of magnetic field). This observation, equivalent to  $D \approx 0.09 \text{ cm}^{-1}$ , confirms that the principal axis of the ZFS ( $Z$ ) is parallel to the molecular  $C_3$  axis. At  $\theta = 0^\circ$  there is no mixing of the  $M_S$  states since  $E = 0$ . Thus, each energy level  $\varphi$  is described by a pure  $M_S$  state  $|\varphi\rangle = |S, M_S\rangle$ —i.e., in zero field the ground state is  $|6, 0\rangle$  (because  $D$  is positive), the first excited states are  $|6, \pm 1\rangle$ , and so on. These levels vary linearly in energy with magnetic field strength (Fig. 3). Transitions are observed between the consecutive levels ( $\Delta M_S = \pm 1$ ) because of the selection rules given by Eq. (3). Only eight of the 2S allowed transitions are observed. The other four lie at “negative” magnetic fields at the  $X$  band. At higher frequencies, and hence magnetic fields, all 12 allowed transitions have been observed.<sup>11</sup>

By contrast, no transitions are observed in the parallel-mode EPR spectrum at  $\theta = 0^\circ$  (Fig. 2) since no two energy levels contain admixtures from the same  $M_S$  state to satisfy Eq. (5). Parallel-mode transitions are totally forbidden at this orientation of the static field. When  $\theta \neq 0^\circ$ , EPR spectra are observed in both parallel and perpendicular modes (Fig. 2).

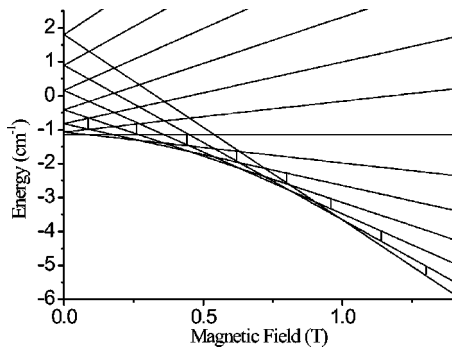


FIG. 3. Energy level diagram of  $\text{Cr}_{12}$  at  $\theta=0^\circ$ . Allowed perpendicular-mode EPR transitions ( $\nu=9.62$  GHz) are marked. No parallel-mode EPR transitions are allowed.

These spectra are complex due to the nonlinear variation of the energy levels in low magnetic fields at X-band (Fig. 4). At higher frequencies, and magnetic fields, much simpler perpendicular-mode spectra are observed.<sup>10,11</sup> This nonlinearity reflects the mixing of the  $M_S$  states that arises from off-diagonal terms in the spin Hamiltonian. In the strict axial symmetry of  $\text{Cr}_{12}$  and the spin Hamiltonian (1), the only off-diagonal terms arise from the Zeeman term. For a given orientation  $\theta$  of the magnetic field  $B_0$  with respect to the molecular Z axis, Eq. (1) can be written as

$$\hat{H} = \beta \cdot g_{zz} \cdot \mathbf{B}_0 \cdot \hat{S}_z \cdot \cos(\theta) + \beta \cdot g_{xx} \cdot \mathbf{B}_0 \cdot \hat{S}_x \cdot \sin(\theta) + D \left[ \hat{S}_z^2 - \frac{1}{3} S(S+1) \right]. \quad (8)$$

Thus, mixing is the result of the action of the transverse spin operator  $\hat{S}_x$  on the zero-order eigenfunctions and the magnitude of the related off-diagonal terms depends on  $\theta$  and the magnitude of  $B_0$ . The resulting wave functions can be described by linear combinations of the  $M_S$  states:

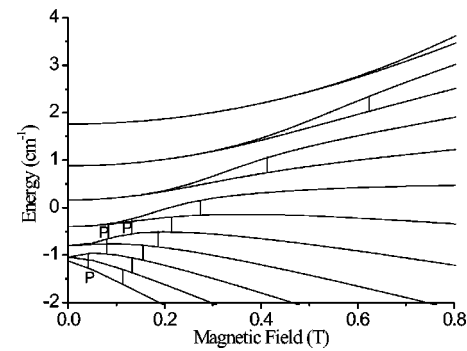


FIG. 4. Energy level diagram of  $\text{Cr}_{12}$  at  $\theta=90^\circ$ . Allowed perpendicular ( $\nu=9.62$  GHz) and parallel (labeled “P”) mode ( $\nu=9.43$  GHz) EPR transitions are marked.

$$|\varphi_{(i)}\rangle = \sum_{M_S=-S}^S c_{iM_S} |S, M_S\rangle. \quad (9)$$

The coefficients  $c$  depend on the orientation and strength of the static magnetic field, and are given by diagonalization of the appropriate secular determinant.

Thus, when  $\theta \neq 0^\circ$  it is possible for both equations (3) and (5) to be satisfied, and EPR transitions to be allowed in both perpendicular and parallel modes, albeit with different transition probabilities (see below). At some orientations between  $\theta=0$  and  $90^\circ$  the same transitions have significant intensity in both modes, for example, the spectra at  $15^\circ$  are remarkably similar (Fig. 2).

At  $\theta=90^\circ$ , however, the only significantly intense transitions in the parallel-mode spectrum are at low field, below ca. 1500 G, while in perpendicular mode the most intense transitions are at resonance fields greater than ca. 1500 G. The transition probabilities are proportional to the square of the appropriate matrix elements, given in Eq. (3) for parallel mode and Eq. (5) for perpendicular mode. The first intense parallel-mode transition for  $\theta=90^\circ$  is at 405 G and is between energy levels  $\varphi_2$  and  $\varphi_4$ —this transition is forbidden

TABLE I. Composition of the  $S=6$  ground state of  $\text{Cr}_{12}$  for an external field of 405 G at  $\theta=90^\circ$ .

Energy level	$E$ (cm <sup>-1</sup> )	$M_S$ states												
		$ 6\rangle$	$ 5\rangle$	$ 4\rangle$	$ 3\rangle$	$ 2\rangle$	$ 1\rangle$	$ 0\rangle$	$ -1\rangle$	$ -2\rangle$	$ -3\rangle$	$ -4\rangle$	$ -5\rangle$	$ -6\rangle$
$\varphi_1$	-1.294	0.00	0.00	0.00	0.01	-0.12	0.45	-0.75	0.45	-0.12	0.01	0.00	0.00	0.00
$\varphi_2$	-1.115	0.00	0.00	0.00	0.04	-0.27	0.65	0.00	-0.65	0.27	-0.04	0.00	0.00	0.00
$\varphi_3$	-0.985	0.00	0.00	-0.01	0.07	-0.35	0.42	0.62	0.42	-0.35	0.07	-0.01	0.00	0.00
$\varphi_4$	-0.801	0.00	0.00	-0.02	0.18	-0.62	-0.28	0.00	0.28	0.62	-0.18	0.02	0.00	0.00
$\varphi_5$	-0.786	0.00	0.00	0.02	-0.18	0.58	0.34	0.22	0.34	0.58	-0.18	0.02	0.00	0.00
$\varphi_6$	-0.398	0.00	0.01	-0.12	0.67	0.19	0.03	0.00	-0.03	-0.19	-0.67	0.12	-0.01	0.00
$\varphi_7$	-0.398	0.00	0.01	-0.12	0.67	0.19	0.03	0.01	0.03	0.19	0.67	-0.12	0.01	0.00
$\varphi_8$	0.172	0.00	0.08	-0.69	-0.12	-0.01	0.00	0.00	0.00	0.01	0.12	0.69	-0.08	0.00
$\varphi_9$	0.172	0.00	0.08	-0.69	-0.12	-0.01	0.00	0.00	0.00	-0.01	-0.12	-0.69	0.08	0.00
$\varphi_{10}$	0.908	-0.05	0.70	0.08	0.01	0.00	0.00	0.00	0.00	0.00	-0.01	-0.08	-0.70	0.05
$\varphi_{11}$	0.908	-0.05	0.70	0.08	0.01	0.00	0.00	0.00	0.00	0.00	0.01	0.08	0.70	-0.05
$\varphi_{12}$	1.809	0.95	0.07	0.00	0.00	0.00	0.00	0.00	0.00	0.00	0.00	0.00	-0.02	-0.30
$\varphi_{13}$	1.809	-0.30	-0.02	0.00	0.00	0.00	0.00	0.00	0.00	0.00	0.00	-0.07	-0.07	-0.95

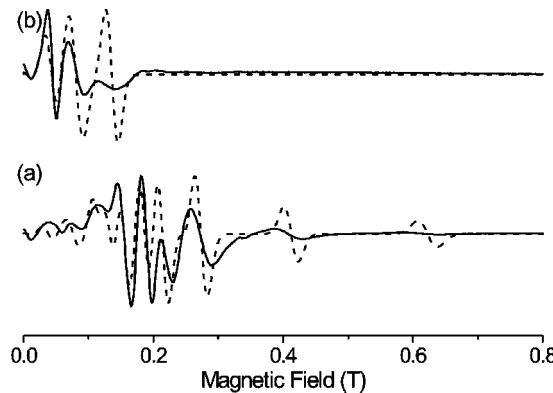


FIG. 5. Single-crystal X-band EPR spectra of  $\text{Cr}_{12}$  at  $\theta=90^\circ$  and 5 K: (a) perpendicular mode, (b) parallel mode. Dashed lines are simulated spectra. In order to compare the relative intensities of EPR transitions and exclude different broadening effects the same bandwidth was used for all transitions.

in perpendicular mode. The compositions of the 13 energy levels at this field and orientation are in Table I. The ground state ( $\varphi_2$ ) has significant contributions from  $M_S = \pm 1, \pm 2$  while the excited state ( $\varphi_4$ ) has major contributions from  $M_S = \pm 1, \pm 2, \pm 3$ . Worked examples of evaluating the appropriate matrix elements (3) and (5) are in Appendixes (A) and (B). (Note the small difference in resonance fields for parallel and perpendicular modes for the same transition, due to the slightly different excitation frequencies of the two modes.) Thus, there is a significant nonzero transition probability for this transition in parallel mode, but in perpendicular mode the matrix elements cancel out to zero—note that the signs of the coefficients  $c$  are crucial as well as their magnitude. The resulting calculated transition probabilities are  $P_{(2,4,\parallel)} = 0.1284$  for parallel mode excitation (note that the subscripts refer to the energy levels involved in the transition), but  $P_{(2,4,\perp)} = 0$  for the equivalent transition in perpendicular mode (experimental and simulated spectra are shown in Fig. 5). Thus this transition is much more intense in

the parallel mode spectrum.

There are also many allowed perpendicular mode transitions at  $\theta=90^\circ$  that are forbidden in parallel mode. For example, the intense transition at 2741 G in perpendicular mode is between energy levels  $\varphi_6$  and  $\varphi_7$ : the composition of the 13 energy levels at this field and orientation is in Table II. The ground state ( $\varphi_6$ ) has significant contributions from  $M_S = \pm 1, \pm 2, \pm 4$ , and  $\pm 5$  while the excited state ( $\varphi_7$ ) has major contributions from  $M_S = 0, \pm 1, \pm 2, \pm 3, \pm 4$ , and  $\pm 5$ . By similar arguments these lead to transition probabilities of  $P_{(6,7,\perp)} = 0.1165$  and  $P_{(6,7,\parallel)} = 0$ .

Table III and Table IV give the coefficients for the 13 zero-order components of the eigenfunctions at  $\theta=90^\circ$  at the resonance fields of all the experimentally observed transitions (see Figs. 4 and 5) for perpendicular and parallel modes, respectively. The transition probabilities for the other intense transitions in the parallel mode spectrum are  $P_{(3,5,\parallel)} = 0.1184$  at 803 G,  $P_{(5,7,\parallel)} = 0.1528$  at 831 G (we do not resolve these transitions separately in the experimental spectrum), and  $P_{(5,7,\perp)} = 0.1436$  at 1325 G (perpendicular mode probabilities all zero). The intense perpendicular-mode transitions [see Fig. 5(a)] are at 385, 763, 1138, 1330, 1558, 1863, 2140, 2741, 4129, 6235, and 9727 G and have probabilities of  $P_{(2,5,\perp)} = 0.0504$ ,  $P_{(5,6,\perp)} = 0.0765$ ,  $P_{(1,2,\perp)} = 0.1045$ ,  $P_{(2,3,\perp)} = 0.1505$ ,  $P_{(3,4,\perp)} = 0.1622$ ,  $P_{(4,5,\perp)} = 0.1529$ ,  $P_{(5,6,\perp)} = 0.1387$ ,  $P_{(6,7,\perp)} = 0.1165$ ,  $P_{(8,9,\perp)} = 0.0848$ ,  $P_{(10,11,\perp)} = 0.0591$ , and  $P_{(12,13,\perp)} = 0.0279$ , respectively. The corresponding probabilities in parallel mode are all zero, i.e., these transitions are allowed only in perpendicular mode.

Powder spectra recorded in parallel and perpendicular modes are given in Fig. 6. Because of the axial symmetry of  $\text{Cr}_{12}$ , the powder spectra are dominated by transitions arising from orientations of the molecules perpendicular to the unique ( $Z$ ) axis (i.e., in the  $XY$  plane). This effect is further emphasized in the parallel-mode powder spectrum, where transitions at fields parallel to the  $Z$  axis are forbidden (see

TABLE II. Composition of the  $S=6$  ground state of  $\text{Cr}_{12}$  for an external field of 2741 G at  $\theta=90^\circ$ .

Energy level	$E$ (cm $^{-1}$ )	$M_S$ states												
		$ 6\rangle$	$ 5\rangle$	$ 4\rangle$	$ 3\rangle$	$ 2\rangle$	$ 1\rangle$	$ 0\rangle$	$ {-1}\rangle$	$ {-2}\rangle$	$ {-3}\rangle$	$ {-4}\rangle$	$ {-5}\rangle$	$ {-6}\rangle$
$\varphi_1$	-2.499	0.00	-0.01	0.03	-0.11	0.28	-0.49	0.59	-0.49	0.28	-0.11	0.03	-0.01	0.00
$\varphi_2$	-1.957	0.00	0.02	-0.09	0.28	-0.48	0.43	0.00	-0.43	0.48	-0.28	0.09	-0.02	0.00
$\varphi_3$	-1.450	0.01	-0.05	0.20	-0.43	0.41	0.08	-0.44	0.08	0.41	-0.43	0.20	-0.05	0.01
$\varphi_4$	-0.980	-0.02	0.11	-0.33	0.45	-0.05	-0.42	0.00	0.42	0.05	-0.45	0.33	-0.11	0.02
$\varphi_5$	-0.550	0.03	-0.18	0.42	-0.28	-0.33	0.15	0.42	0.15	-0.33	-0.28	0.42	-0.18	0.03
$\varphi_6$	-0.162	-0.06	0.26	-0.42	-0.02	0.38	0.33	0.00	-0.33	-0.38	0.02	0.42	-0.26	0.06
$\varphi_7$	0.160	-0.08	0.30	-0.32	-0.25	0.10	0.36	0.45	0.36	0.10	-0.25	-0.32	0.30	-0.08
$\varphi_8$	0.496	0.13	-0.38	0.17	0.41	0.34	0.17	0.00	-0.17	-0.34	-0.41	-0.17	0.38	-0.13
$\varphi_9$	0.585	-0.11	0.32	-0.09	-0.33	-0.35	-0.32	-0.30	-0.32	-0.35	-0.33	-0.09	0.32	-0.11
$\varphi_{10}$	1.164	-0.29	0.43	0.41	0.23	0.10	0.04	0.00	-0.04	-0.10	-0.23	-0.41	-0.43	0.29
$\varphi_{11}$	1.167	-0.29	0.43	0.41	0.23	0.11	0.05	0.04	0.05	0.11	0.23	0.41	0.43	-0.29
$\varphi_{12}$	2.014	-0.63	-0.30	-0.11	-0.03	-0.01	0.00	0.00	0.00	0.01	0.03	0.11	0.30	0.63
$\varphi_{13}$	2.014	0.63	0.30	0.11	0.03	0.01	0.00	0.00	0.00	0.01	0.03	0.11	0.30	0.63

TABLE III. Assignment of observed transitions in perpendicular-mode X-band EPR spectra of Cr<sub>12</sub> at  $\theta=90^\circ$ .

Resonant field (G)		Levels	$ 6\rangle$	$ 5\rangle$	$ 4\rangle$	$ 3\rangle$	$ 2\rangle$	$ 1\rangle$	$ 0\rangle$	$ -1\rangle$	$ -2\rangle$	$ -3\rangle$	$ -4\rangle$	$ -5\rangle$	$ -6\rangle$
385	$\varphi_2$	0.00	0.00	0.00	0.04	-0.27	0.65	0.00	-0.65	0.27	-0.04	0.00	0.00	0.00	
	$\varphi_5$	0.00	0.00	0.02	-0.17	0.59	0.32	0.20	0.32	0.59	-0.17	0.02	0.00	0.00	
763	$\varphi_5$	0.00	0.01	-0.06	0.28	-0.32	-0.46	-0.45	-0.46	-0.32	0.28	-0.06	0.01	0.00	
	$\varphi_6$	0.00	-0.03	0.22	-0.58	-0.32	-0.10	0.00	0.10	0.32	0.58	-0.22	0.03	0.00	
1138	$\varphi_1$	0.00	0.00	0.01	-0.06	0.21	-0.49	0.65	-0.49	0.21	-0.06	0.01	0.00	0.00	
	$\varphi_2$	0.00	0.00	0.03	-0.16	0.44	-0.53	0.00	0.53	-0.44	0.16	-0.03	0.00	0.00	
1330	$\varphi_2$	0.00	0.00	0.04	-0.18	0.45	-0.51	0.00	0.51	-0.45	0.18	-0.04	0.00	0.00	
	$\varphi_3$	0.00	0.01	-0.09	0.32	-0.51	0.04	0.50	0.04	-0.51	0.32	-0.09	0.01	0.00	
1558	$\varphi_3$	0.00	-0.02	0.11	-0.35	0.50	-0.01	-0.48	-0.01	0.50	-0.35	0.11	-0.02	0.00	
	$\varphi_4$	0.00	-0.04	0.20	-0.46	0.25	0.44	0.00	-0.44	-0.25	0.46	-0.20	0.04	0.00	
1863	$\varphi_4$	0.01	-0.06	0.24	-0.47	0.18	0.44	0.00	-0.44	-0.18	0.47	-0.24	0.06	-0.01	
	$\varphi_5$	-0.01	0.09	-0.33	0.40	0.21	-0.26	-0.47	-0.26	0.21	0.40	-0.33	0.09	-0.01	
2140	$\varphi_5$	-0.02	0.12	-0.37	0.36	0.26	-0.22	-0.45	-0.22	0.26	0.36	-0.37	0.12	-0.02	
	$\varphi_6$	0.03	-0.18	0.42	-0.13	-0.43	-0.31	0.00	0.31	0.43	0.13	-0.42	0.18	-0.03	
2741	$\varphi_6$	-0.06	0.26	-0.42	-0.02	0.38	0.33	0.00	-0.33	-0.38	0.02	0.42	-0.26	0.06	
	$\varphi_7$	-0.08	0.30	-0.32	-0.25	0.10	0.36	0.45	0.36	0.10	-0.25	-0.32	0.30	-0.08	
4129	$\varphi_8$	-0.24	0.39	0.12	-0.27	-0.38	-0.25	0.00	0.25	0.38	0.27	-0.12	-0.39	0.24	
	$\varphi_9$	-0.25	0.28	0.24	-0.03	-0.25	-0.38	-0.42	-0.38	-0.25	-0.03	0.24	0.28	-0.25	
6235	$\varphi_{10}$	-0.42	-0.12	0.21	0.35	0.33	0.19	0.00	-0.19	-0.33	-0.35	-0.21	0.12	0.42	
	$\varphi_{11}$	0.33	0.20	-0.02	-0.20	-0.31	-0.37	-0.38	-0.37	-0.31	-0.20	-0.02	0.20	0.33	
9727	$\varphi_{12}$	0.21	0.33	0.38	0.35	0.26	0.14	0.00	-0.14	-0.26	-0.35	-0.38	-0.33	-0.21	
	$\varphi_{13}$	0.11	0.20	0.26	0.31	0.33	0.34	0.35	0.34	0.33	0.31	0.26	0.20	0.11	

above), and all the intense features in the powder spectrum are due to transitions in the XY plane [ $\theta=90^\circ$ ; see Figs. 5(b) and 6(b)].

The work above shows that parallel-mode EPR spectroscopy of a high-spin, non-Kramers system not only has sufficient sensitivity to detect transitions ( $\leq$  an order of magnitude compared to perpendicular mode spectra), but also produces distinct transitions from those excited by conventional perpendicular mode, and therefore will be valuable in the study of high-spin clusters such as SMMs. For instance, Fig. 4 and Table III show the (static) field dependence of the eigenstates and the evolution of the eigenvectors in the field. This reveals how, in principle, a selective connection be-

tween states might be achieved by orientation selection of the oscillating field and consequent variations in the components of the total transition probability.

This suggests possible additional uses of EPR in the study and exploitation of high-spin clusters. For example, Wernsdorfer *et al.* have proposed that certain SMMs, where the clusters themselves are weakly intermolecularly exchange coupled (“exchange biased”), could be exploited as qubits in quantum computing.<sup>8(a)</sup> Specifically, they discuss a discrete dimer of tetrametallic manganese SMM clusters [Mn<sub>4</sub>O<sub>3</sub>Cl<sub>4</sub>(O<sub>2</sub>CEt)<sub>3</sub>(py)<sub>3</sub>]<sub>2</sub> (py indicates pyridine and Et an ethyl group), where the weak exchange between the two  $S=9/2$  ground-state molecules provides a mechanism for the

TABLE IV. Assignment of observed transitions in parallel-mode X-band EPR spectra of Cr<sub>12</sub> at  $\theta=90^\circ$ .

Resonant field (G)		Levels	$ 6\rangle$	$ 5\rangle$	$ 4\rangle$	$ 3\rangle$	$ 2\rangle$	$ 1\rangle$	$ 0\rangle$	$ -1\rangle$	$ -2\rangle$	$ -3\rangle$	$ -4\rangle$	$ -5\rangle$	$ -6\rangle$
405	$\varphi_2$	0.00	0.00	0.00	0.04	-0.27	0.65	0.00	-0.65	0.27	-0.04	0.00	0.00	0.00	
	$\varphi_4$	0.00	0.00	-0.02	0.18	-0.62	-0.28	0.00	0.28	0.62	-0.18	0.02	0.00	0.00	
415	$\varphi_1$	0.00	0.00	0.00	0.02	-0.12	0.46	-0.75	0.46	-0.12	0.02	0.00	0.00	0.00	
	$\varphi_3$	0.00	0.00	-0.01	0.07	-0.36	0.42	0.62	0.42	-0.36	0.07	-0.01	0.00	0.00	
803	$\varphi_3$	0.00	0.00	0.04	-0.21	0.51	-0.18	-0.56	-0.18	0.51	-0.21	0.04	0.00	0.00	
	$\varphi_5$	0.00	0.01	-0.07	0.30	-0.29	-0.46	-0.47	-0.46	-0.29	0.30	-0.07	0.01	0.00	
831	$\varphi_5$	0.00	0.01	-0.07	0.30	-0.29	-0.46	-0.47	-0.46	-0.29	0.30	-0.07	0.01	0.00	
	$\varphi_7$	0.00	-0.03	0.23	-0.56	-0.34	-0.14	-0.08	-0.14	-0.34	-0.56	0.23	-0.03	0.00	
1325	$\varphi_5$	0.00	-0.04	0.21	-0.42	-0.02	0.38	0.51	0.38	-0.02	-0.42	0.21	-0.04	0.00	
	$\varphi_7$	0.01	-0.08	0.30	-0.30	-0.41	-0.33	-0.28	-0.33	-0.41	-0.30	0.30	-0.08	0.01	

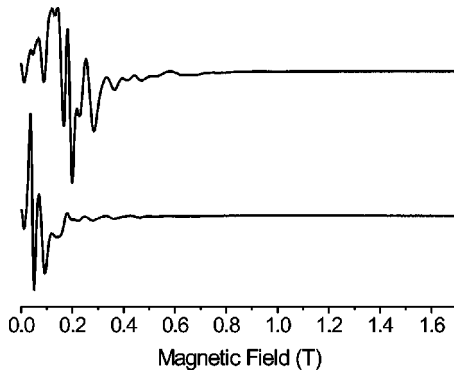


FIG. 6. (Top) perpendicular- and (bottom) parallel-mode X-band EPR spectra of a powdered sample of  $\text{Cr}_{12}$  at 5 K.

coherent superposition of levels. The eigenfunctions of the dimer at  $\theta=0^\circ$  are linear combinations of the pure  $M_S$  states of the individual tetramers, mixed by the exchange “bias,” as recently elegantly demonstrated by Hill *et al.* via high-

frequency (perpendicular-mode) EPR, where spectral splittings of otherwise degenerate transitions derive from the transverse component of the exchange.<sup>8(b)</sup> EPR thus provides a direct measure of the strength of the intermolecular exchange bias. However, the  $\Delta M_S = \pm 1$  selection rule limits the number of possible transitions that can be excited. The use of parallel-mode EPR would allow excitation to states connected to the ground state via  $\Delta M_S = 0$  (these transitions would become allowed at  $\theta=0^\circ$  via the exchange bias interaction), and hence provide complementary information to perpendicular-mode excitation on the nature of the biasing phenomenon. Indeed, X-band EPR may be particularly useful here, because Hill *et al.*<sup>8(b)</sup> have estimated that the exchange biasing in this particular example leads to separation of otherwise degenerate pairs of levels by ca. 9 GHz.

#### ACKNOWLEDGMENTS

This work has been supported by the EPSRC, INTAS, and The Royal Society.

#### APPENDIX A: EVALUATION OF MATRIX ELEMENTS FOR $\varphi_2 \rightarrow \varphi_4$ IN PARALLEL-MODE EPR AT 405 G AND $\theta=90^\circ$

$$P_{(2,4,\parallel)} \propto \left| \frac{1}{2} \langle \varphi(4) | (\hat{S}_+ + \hat{S}_-) | \varphi(2) \rangle \right|^2,$$

$$|\varphi(2)\rangle = 0.04 \cdot |3\rangle - 0.27 \cdot |2\rangle + 0.65 \cdot |1\rangle - 0.65 \cdot |-1\rangle + 0.27 \cdot |-2\rangle - 0.04 \cdot |-3\rangle,$$

$$|\varphi(4)\rangle = -0.02 \cdot |4\rangle + 0.18 \cdot |3\rangle - 0.62 \cdot |2\rangle - 0.28 \cdot |1\rangle + 0.28 \cdot |-1\rangle + 0.62 \cdot |-2\rangle - 0.18 \cdot |-3\rangle + 0.02 \cdot |-4\rangle,$$

$$\begin{aligned} P_{(2,4,\parallel)} &\propto \left| \frac{1}{2} \cdot [ -0.02 \cdot 0.04 \cdot \langle 4 | \hat{S}_+ | 3 \rangle - 0.18 \cdot 0.27 \cdot \langle 3 | \hat{S}_+ | 2 \rangle - 0.62 \cdot 0.65 \cdot \langle 2 | \hat{S}_+ | 1 \rangle + 0.28 \cdot 0.27 \cdot \langle -1 | \hat{S}_+ | -2 \rangle \right. \\ &\quad \left. - 0.62 \cdot 0.04 \cdot \langle -2 | \hat{S}_+ | -3 \rangle - 0.02 \cdot 0.04 \cdot \langle -4 | \hat{S}_- | -3 \rangle - 0.18 \cdot 0.27 \cdot \langle -3 | \hat{S}_- | -2 \rangle - 0.62 \cdot 0.65 \cdot \langle -2 | \hat{S}_- | -1 \rangle \right. \\ &\quad \left. + 0.28 \cdot 0.27 \cdot \langle 1 | \hat{S}_- | 2 \rangle - 0.62 \cdot 0.04 \cdot \langle 2 | \hat{S}_- | 3 \rangle ] \right|^2, \end{aligned}$$

$$\begin{aligned} P_{(2,4,\parallel)} &\propto \left| \frac{1}{2} \cdot [ -0.0008 \cdot (\langle 4 | \hat{S}_+ | 3 \rangle + \langle -4 | \hat{S}_- | -3 \rangle) - 0.0486 \cdot (\langle 3 | \hat{S}_+ | 2 \rangle + \langle -3 | \hat{S}_- | -2 \rangle) - 0.403 \cdot (\langle 2 | \hat{S}_+ | 1 \rangle \right. \\ &\quad \left. + \langle -2 | \hat{S}_- | -1 \rangle) + 0.0756 \cdot (\langle -1 | \hat{S}_+ | -2 \rangle + \langle 1 | \hat{S}_- | 2 \rangle) - 0.0248 \cdot (\langle -2 | \hat{S}_+ | -3 \rangle + \langle 2 | \hat{S}_- | 3 \rangle) ] \right|^2, \end{aligned}$$

$$\begin{aligned} P_{(2,4,\parallel)} &\propto \left| -0.0008 \cdot 2.74 \cdot (\langle 4 | 4 \rangle + \langle -4 | -4 \rangle) - 0.0486 \cdot 3.00 \cdot (\langle 3 | 3 \rangle + \langle -3 | -3 \rangle) - 0.403 \cdot 3.16 \cdot (\langle 2 | 2 \rangle + \langle -2 | -2 \rangle) \right. \\ &\quad \left. + 0.0756 \cdot 3.24 \cdot (\langle -1 | -1 \rangle + \langle 1 | 1 \rangle) - 0.0248 \cdot 3.24 \cdot (\langle -2 | -2 \rangle + \langle 2 | 2 \rangle) \right|^2, \end{aligned}$$

$$P_{(2,4,\parallel)} \propto 6.32, \quad P_{(2,4,\parallel)} \neq 0.$$

#### APPENDIX B: EVALUATION OF MATRIX ELEMENTS FOR $\varphi_2 \rightarrow \varphi_4$ IN PERPENDICULAR MODE EPR AT 429 G AND $\theta=90^\circ$

$$P_{(2,4,\perp)} \propto |\langle \varphi(4) | \hat{S}_z | \varphi(2) \rangle|^2,$$

$$|\varphi(2)\rangle = 0.05 \cdot |3\rangle - 0.28 \cdot |2\rangle + 0.65 \cdot |1\rangle - 0.65 \cdot |-1\rangle + 0.28 \cdot |-2\rangle - 0.05 \cdot |-3\rangle,$$

$$|\varphi(4)\rangle = -0.02 \cdot |4\rangle + 0.19 \cdot |3\rangle - 0.62 \cdot |2\rangle - 0.29 \cdot |1\rangle + 0.29 \cdot |-1\rangle + 0.62 \cdot |-2\rangle - 0.19 \cdot |-3\rangle + 0.02 \cdot |-4\rangle,$$

$$\begin{aligned} P_{(2,4,\perp)} &\propto \left| 0.19 \cdot 0.05 \cdot \langle 3 | \hat{S}_z | 3 \rangle + 0.62 \cdot 0.28 \cdot \langle 2 | \hat{S}_z | 2 \rangle - 0.29 \cdot 0.65 \cdot \langle 1 | \hat{S}_z | 1 \rangle - 0.29 \cdot 0.65 \cdot \langle -1 | \hat{S}_z | -1 \rangle \right. \\ &\quad \left. + 0.62 \cdot 0.28 \cdot \langle -2 | \hat{S}_z | -2 \rangle + 0.19 \cdot 0.05 \cdot \langle -3 | \hat{S}_z | -3 \rangle \right|^2, \end{aligned}$$

$$P_{(2,4,\perp)} \propto |0.0095 \cdot (\langle 3|\hat{S}_z|3\rangle + \langle -3|\hat{S}_z|-3\rangle) + 0.1736 \cdot (\langle 2|\hat{S}_z|2\rangle + \langle -2|\hat{S}_z|-2\rangle) - 0.1885 \cdot (\langle 1|\hat{S}_z|1\rangle + \langle -1|\hat{S}_z|-1\rangle)|^2,$$

$$P_{(2,4,\perp)} \propto |0.0095 \cdot (3 \cdot \langle 3|3\rangle - 3 \cdot \langle -3|-3\rangle) + 0.1736 \cdot (2 \cdot \langle 2|2\rangle - 2 \cdot \langle -2|-2\rangle) - 0.1885 \cdot (\langle 1|1\rangle - \langle -1|-1\rangle)|^2,$$

$$P_{(2,4,\perp)} \propto |0.0095 \cdot (3 - 3) + 0.1736 \cdot (2 - 2) - 0.1885 \cdot (1 - 1)|^2,$$

$$P_{(2,4,\perp)} = 0.$$

\*Fax: +44-161-275-4616. E-mail address: eric.mcinnes@man.ac.uk.

<sup>1</sup>A. Abragam and B. Bleaney, *Electron Paramagnetic Resonance of Transition Ions* (Clarendon Press, Oxford, 1970).

<sup>2</sup>For example, (a) D.J.B. Hunter, V.S. Oganesyan, J.C. Salerno, C.S. Butler, W.J. Ingledew, and A.J. Thomson, *Biophys. J.* **78**, 439 (2000); (b) K.A. Campbell, E. Yikilmaz, C.V. Grant, W. Gregor, A.-F. Miller, and R.D. Britt, *J. Am. Chem. Soc.* **121**, 4714 (1999).

<sup>3</sup>M.P. Hendrich and P.G. Debrunner, *Biophys. J.* **56**, 489 (1989).

<sup>4</sup>W.R. Hagen, *Adv. Inorg. Chem. Radiochem.* **38**, 165 (1992); A.J. Pierik, W.R. Hagen, W.R. Dunhem, and R.H. Sands, *Eur. J. Biochem.* **206**, 705 (1992); S.J. Yoo, H. Angove, B.K. Burgess, M. P. Hendrich, and E. Münck, *J. Am. Chem. Soc.* **121**, 2534 (1999).

<sup>5</sup>K.A. Campbell, D.A. Force, P.J. Nixon, F. Dole, B.A. Diner, and R.D. Britt, *J. Am. Chem. Soc.* **122**, 3754 (2000).

<sup>6</sup>(a) R. Sessoli, H.-L. Tsai, A.R. Schake, S. Wang, J. B. Vincent, K. Folting, D. Gatteschi, G. Christou, and D.N. Hendrickson, *J. Am. Chem. Soc.* **115**, 1804 (1993); (b) R. Sessoli, D. Gatteschi,

A. Caneschi, and M. Novak, *Nature (London)* **365**, 141 (1993).

<sup>7</sup>M.N. Leuenberger and D. Loss, *Nature (London)* **410**, 789 (2001).

<sup>8</sup>(a) W. Wernsdorfer, N. Aliaga-Alcalde, D.N. Hendrickson, and G. Christou, *Nature (London)* **416**, 406 (2002); (b) S. Hill, R.S. Edwards, N. Aliaga-Alcalde, and G. Christou, *Science* **302**, 1015 (2003).

<sup>9</sup>A.L. Barra, L.-C. Brunel, D. Gatteschi, L. Pardi, and R. Sessoli, *Acc. Chem. Res.* **31**, 460 (1998).

<sup>10</sup>A.S. Batsanov, G.A. Timco, N.V. Struchkov, N.V. Gérbeléu, and K.M. Indrichan, *Koord. Khim.* **17**, 662 (1991); F.E. Mabbs, E.J.L. McInnes, M. Murrie, S. Parsons, G.M. Smith, C.C. Wilson, and R.E.P. Winpenny, *Chem. Commun. (Cambridge)* **1999**, 643.

<sup>11</sup>D. Collison, V.S. Oganesyan, S. Piligkos, A.J. Thomson, R.E.P. Winpenny, and E.J.L. McInnes, *J. Am. Chem. Soc.* **125**, 1168 (2003); D. Collison, M. Murrie, V.S. Oganesyan, S. Piligkos, N.R.J. Poolton, G. Rajaraman, G.M. Smith, A.J. Thomson, G.A. Timco, W. Wernsdorfer, R.E.P. Winpenny, and E.J.L. McInnes, *Inorg. Chem.* **42**, 5293 (2003).